Acta Pharmaceutica Sinica B 2018;8(1):74–84

Chinese Pharmaceutical Association
Institute of Materia Medica, Chinese Academy of Medical Sciences

Acta Pharmaceutica Sinica B

www.elsevier.com/locate/apsb
www.sciencedirect.com

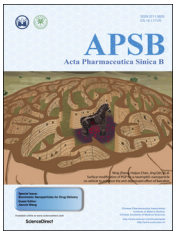

ORIGINAL ARTICLE

Biomimetic albumin-modified gold nanorods for photothermo-chemotherapy and macrophage polarization modulation

Dongdong Li[a,b], Meng Zhang[a], Fan Xu[a,b], Yingzhi Chen[a], Binfan Chen[a], Ya Chang[a,b], Huihai Zhong[a,c], Hongyue Jin[a], Yongzhuo Huang[a,*]

[a]*Shanghai Institute of Materia Medica, Chinese Academy of Sciences, Shanghai 201203, China*
[b]*Nano Sci-Tech Institute, University of Science and Technology of China, Suzhou 215123, China*
[c]*Shanghai University College of Sciences, Shanghai 200444, China*

Received 24 June 2017; received in revised form 2 August 2017; accepted 25 August 2017

KEY WORDS

Photothermal therapy;
Paclitaxel;
Combination therapy;
Gold nanorods;
Albumin;
Tumor-associated macrophage

Abstract Nanotechnology-based photothermal therapy has attracted great attention in the past decade. Nevertheless, photothermal therapy has some inherent drawbacks, such as the uneven heat production and limited laser penetration, often leading to insufficient treatment outcomes. Here, we developed a combination strategy to improve cancer therapy. The biomimetic albumin-modified gold nanorods (AuNRs) were prepared with incorporation of paclitaxel (PTX). This therapeutic system was characterized by several features. First, the albumin modification enhanced the biocompatibility and colloidal stability. Second, the surface-coated albumin promoted cellular uptake *via* the albumin-binding protein pathway. Third, PTX was incorporated *via* hydrophobic interaction between PTX and the albumin lipophilic domain. Fourth, the system can be used for combined photothermo-chemotherapy for yielding synergistic effects. The antitumor activity of the system was evaluated both *in vitro* and *in vivo* using the HCT116 colon cancer cell and tumor model. The combination therapy was found with an enhanced treatment efficiency and no obvious side effect. Most importantly, the thermal effect was also discovered with the ability to modulate the

*Corresponding author. Tel./fax: +86 21 20231981.
E-mail address: yzhuang@simm.ac.cn (Yongzhuo Huang).

Peer review under responsibility of Institute of Materia Medica, Chinese Academy of Medical Sciences and Chinese Pharmaceutical Association.

http://dx.doi.org/10.1016/j.apsb.2017.09.005

tumor microenvironments and suppress the macrophages polarization towards the M2 pro-tumor phenotype. It could be a mechanism for photothermal immunotherapy. The combination strategy and the system provide a potential method for cancer therapy.

1. Introduction

In the recent decade, photothermal treatment has attracted great attention as a promising avenue for cancer therapy, which makes use of the photothermal effect of the inorganic nanoparticles such as silica/gold nanoshells[1,2], gold nanorods[3,4], gold nanospheres[5,6], gold nanocages[7,8], gold nanostars[9,10], or carbon nanotubes[11,12]. These nanomaterials are administrated by intravenous or intra-tumor injection with subsequent irradiation of laser light to raise the temperature to kill the tumor cells. In photothermal treatments, the temperature in the tumor tissues where the blood vessels are deficient can be 5–8 degrees higher than the normal tissues, thus preferentially eradicating the cancer cells but sparing the healthy cells. Compared to the traditional cancer therapies, the photothermal treatment has great advantages, such as non-invasion, local action, and minor side effects.

Nevertheless, there are some limitations in photothermal treatment, too. For instance, the distribution of nanoparticles in the tumor is highly heterogeneous, and only a tiny fraction of the nanomaterials can reach the deep site of the tumors. In addition, laser beam energy is dramatically reduced after penetrating the tissues and it is at Gaussion distribution pattern, thereby leading to the insufficient photothermal effect deep inside the tumors.

A combination of photothermo-chemotherapy provides a promising method for improving the treatment efficacy[13–15]. The chemo-drugs can be encapsulated into the photothermal nanoparticles, and achieve the tumor targeting effect.

In this study, we developed a nano-system for photothermo-chemotherapy by loading a chemotherapy drug PTX to the albumin-modified AuNRs. Of note, albumin can serve as an efficient carrier of PTX *via* the strong interaction of the hydrophobic PTX binding with the hydrophobic domains of albumin. Another important function of albumin is its preferential uptake by the tumor cells. Albumin-binding proteins, *e.g.*, SPARC (secreted protein acidic and rich in cysteine), are the major pathway for albumin uptake by the tumor cells, which are greatly in need of albumin as a source of amino acids and energy to supply their rapid growth[16]. Therefore, the albumin-based nanoparticles can achieve enhanced tumor uptake *via* the biomimetic transportation mechanism of albumin-binding proteins (*e.g.*, SPARC)[17,18]. Therefore, it was expected that the PTX-loading, albumin-modified AuNRs could benefit from the albumin-mediated biomimetic intracellular delivery.

Thermo-immune responses have been demonstrated to be efficient for cancer therapy[19]. However, the mechanisms have not been understood yet. The tumor-associated macrophages (TAMs) are the major component in the tumor immune microenvironment. In this study, the photothermal effect on the TAMs was investigated.

2. Materials and methods

2.1. Materials

Tetrachloroauric (III) acid trihydrate and 11-mercaptoundecanoic acid (MUA) were purchased from J&K chemical Ltd. (Beijing, China). Bovine serum albumin (BSA) was obtained from RBC Life Sciences (Irving, USA) and PTX was from Melone Pharmaceutical Co., Ltd. (Dalian, China). Tris(hydroxyl methyl)aminomethane ($\geq$ 99.9%) was provided by Beyotime Institute of Biotechnology (Haimen, China). Anti-LC3B antibody was acquired from Cell Signaling Technology, Inc. (Danvers, USA). McCoy's 5A medium and 3-(4,5-dimethylthialzol-2-yl)-2,5-diphenyltetrazolium bromide (MTT) were from Sigma–Aldrich (St. Louis, USA). 1-Ethyl,3-(3-dimethylaminopropyl)carbodiimide (EDC), *N*-hydroxysuccinimide (NHS), cetyl trimethyl ammonium bromide (CTAB), and other reagents were of analytical reagent grade, and purchased from Sinopharm Chemical Reagent Co., Ltd. (Shanghai, China).

2.2. Preparation of CTAB-AuNRs

AuNRs were synthesized by the seed-mediated growth method[20]. Briefly, the $HAuCl_4$ (0.5 mmol/L, 5 mL) aqueous solution was gently mixed with the CTAB solution (0.2 mol/L, 5 mL). Subsequently, with addition of the ice-cold $NaBH_4$ solution (10 mmol/L, 0.6 mL), the mixture was vigorously stirred for 2 min, and then kept at 28 °C for 3 h in darkness to generate the AuNR seeds.

CTAB (0.2 mol/L, 20 mL), silver nitrate (4 mmol/L, 0.8 mL), $HAuCl_4$ (1 mmol/L, 20 mL) were mixed in a flask. The solution was gently mixed, and ascorbic acid (80 mmol/L, 0.28 mL) was added. The mixture was turned from yellow to colorless. Immediately, the AuNR seeds (0.48 mL) were quickly added to the mixed solution above to initiate the growth of AuNRs. The reaction was maintained at 28 °C for 6 h in darkness, the CTAB-AuNRs were generated.

2.3. Preparation of MUA-AuNRs

The MUA-AuNRs were prepared by a round-trip ligand exchange method[21]. First, the CTAB-AuNRs were concentrated (2×10^{-8} –5×10^{-8} mol/L) by centrifugation. Dodecanethiol (DDT) was added to the CTAB-AuNRs aqueous solution to replace the CTAB. The thus-formed DDT-AuNRs were added to acetone. The organic phase was added to the solution of toluene and methanol (1:5). The DDT-AuNRs were collected using centrifugation, and the precipitation was resuspended in toluene by sonication. The DDT-AuNRs in toluene were added to 0.1 mol/L MUA

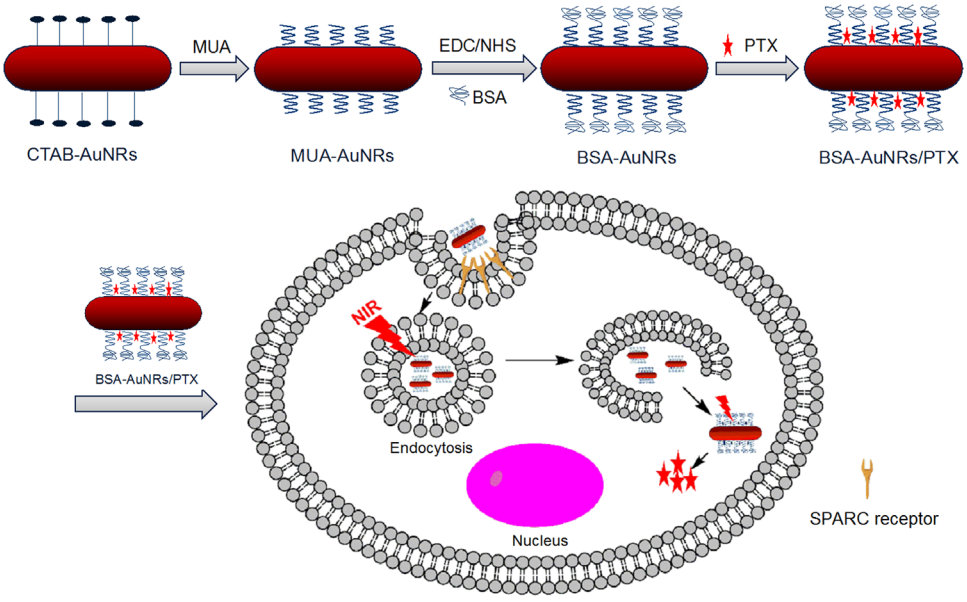

Scheme 1 The process of fabricating BSA-AuNRs. CTAB-AuNRs were synthesized and then CTAB was replaced by MUA through the "round-trip" phase transfer method. BSA was conjugated to MUA *via* EDC/NHS reaction. PTX was incorporated in BSA-AuNRs by hydrophobic interaction.

in toluene. After reflux and vigorously stirring for 15 min at 75 °C, the MUA-AuNRs were formed. They were collected and washed with toluene and isopropanol, successively. Finally, the MUA-AuNRs were resuspended in Tris-borate-EDTA buffer (TBE) for the further experiments.

2.4. *Preparation of BSA-AuNRs and BSA-AuNRs/PTX*

The carboxyl group of the MUA-AuNRs was activated using EDC/NHS. Afterward, BSA (10 mg) was added to the activated NHS-MUA-AuNRs, and reacted for 5 h. The modification of BAS was based on the conjugation of its amino groups to the activated NHS group on the MUA-AuNRs. The BSA-AuNRs was purified by centrifugation and wash for three times.

The PTX/BSA-AuNRs were synthesized by adding PTX (5 mmol/L) to the BSA-AuNRs (50 μg/mL) and stirring for 2 h. Then the PTX/BSA-AuNRs were centrifuged and washed for three times. The PTX loading efficiency was measured by an HPLC method. The PTX/BSA-AuNRs (100 μL) was added to methanol (900 μL). After ultrasound extraction for 10 min and centrifugation, the supernatant was analyzed by HPLC with a reverse-phase C18 column to quantitate PTX. Thermogravimetric analysis (TGA) was also used to characterize the BSA-AuNRs.

2.5. *TEM examination, zeta potential measurement, and vis-spectrum*

The morphologies of AuNRs were detected by transmission electron microscopy (TEM) operated at 200 kV. The zeta potential of the CTAB, MUA, or BSA-coating AuNRs was measured by Zetasizer (Nano-ZS90, Malvern instruments, UK). The spectrum (400–900 nm) was monitored using vis-spectroscopy (Multiscan, Thermo Fisher, USA).

The stability of the PTX/BSA-AuNRs was monitored by measuring the turbidity in the cell culture medium at 380 nm.

2.6. *TGA analysis of BSA-AuNRs*

The thermogravimetric curve of the BSA-AuNRs was measured by thermal gravimetric analyzer (Pyris 1, PerkinElmer, USA). The temperature range was 50–600 °C and the heating rate was 20 °C /min.

2.7. *Measurement of photothermal conversion efficiency*

The photothermal conversion efficiency of the MUA-AuNRs (50 μg/mL) and BSA-AuNRs (50 μg/mL) was monitored using the infrared temperature measurement with irradiation by near infrared laser (NIR, 808 nm, 3 W, 3 min). The temperature–time data was recorded by ThermoX 2.2 and analyzed by GraphPad Prism.

2.8. *Cellular uptake and cell vitality assay*

Human colon cancer cells (HCT116) were cultured in the McCoy's 5 A medium supplemented with 10% (*v*/*v*) FBS and penicillium–streptomycin solution (100 U/mL penicillin, 100 U/mL streptomycin) at 37 °C under 5% CO_2.

For cellular uptake study, the HCT116 cells were planted into the 12-well plates. After 24-h culture, the cells were treated with the rhodamine B-loaded BSA-AuNPs for 45 min. After washed with PBS for 3 times, the cells were subjected for fluorescence microscopic imaging. The PEG-AuNRs prepared by the reaction between PEG-NH_2 and MUA-AuNRs *via* EDC/NHS method was set as control.

The cells were seeded at a density of 5×10^3 cells per well into the 96-well plates. After 24-h incubation, the cells were treated with PTX (dissolved in alcohol/castor oil, 1:1) or the PTX/BSA-AuNRs at various concentrations for another 48 and 72 h. The cell viability was determined by a standard MTT assay. The IC_{50} value was calculated by fitting the dose response–inhibition curve using the GraphPad Prism software.

To examine the effect of the combination of photothermo-chemotherapy, the HCT116 cells were treated as the follow: (1) PTX, (2) BSA-AuNRs+NIR, (3) PTX/BSA-AuNRs, (4) PTX/BSA-AuNRs + NIR, and (5) control group with NIR at

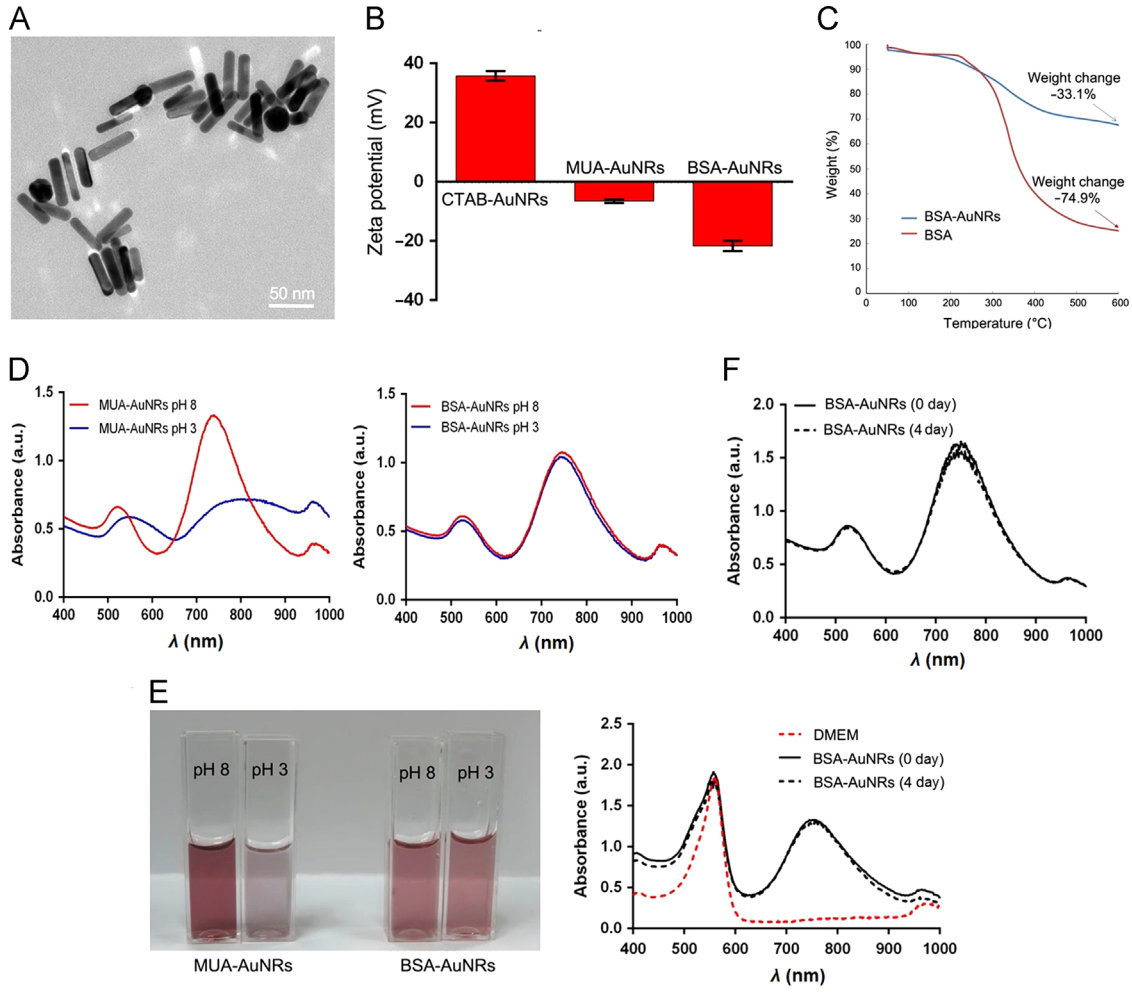

Figure 1 Characterization of the AuNRs. (A) TEM of AuNRs; (B) Zeta potential; (C) The thermogravimetric curve; (D) The spectrum of MUA-AuNRs and BSA-AuNRs at various pH; (E) The color change of the MUA-AuNRs and BSA-AuNRs at various pH; (F) Stability of BSA-AuNRs in water (up panel) and in cell culture medium (bottom panel).

a fixed dose of Au (50 μg/mL) and varying concentration of PTX (1.5, 3, and 6 μg/mL). The cells were incubated with the drugs for 12 h and then washed with PBS for three times before infrared illumination (λ = 808 nm, 3 W, 2 min). After another 12 h, the cell viability was measured by the MTT assay.

2.9. *The effects on cell apoptosis and autophagy*

The HCT116 cells were planted in the 24-well plates. After 24 h, the cells were incubated with the above drugs and then subjected to infrared illumination (5 W, 4 min). The apoptosis of cells was analyzed by the FITC-annexin V kit and flow cytometry.

The cell autophagy was evaluated by the expression level of the autophagy related protein LC3B. The HCT116 cells after treatment with the same procedures as above were subjected to Western blotting assay for measuring the level of LC3B expression.

2.10. *The effect of photothermal therapy on the macrophages polarization*

RAW264.7 macrophages were planted in the 24-well plates and cultured for 24 h. The M2-phenotype macrophages were induced using IL-4 (40 ng/mL), and treated with BSA-AuNRs (20 μg/mL) for 12 or 24 h. After washed using PBS, the cells were treated with laser irradiation (1, 2, or 3 min) and then cultured for another 12 h. The cells were used for Western blotting assay to detect the expression level of mannose receptor and legumain.

2.11. *In vivo chemo-photothermal therapy*

The BALB/c *nu/nu* mice (SPF-level, female, 18 ± 2 g) were purchased from Shanghai SLAC Laboratory Animal Co., Ltd (Shanghai, China). All animal procedures were carried out under the guidelines approved by the Institutional Animal Care and Use Committee of the Shanghai Institute of Materia Medica, Chinese Academy of Sciences. The HCT116 subcutaneous tumor model was developed for the *in vivo* treatment study. When the tumors grew to around 100 mm^3, the mice were divided into 5 groups (n = 5) randomly for the treatments: (1) PBS; (2) PTX; (3) BSA-AuNRs + NIR; (4) PTX/BSA-AuNRs (5) PTX/BSA-AuNRs + NIR. The drug formulations (a dose equal to 1.5 mg/kg of Au and 1 mg/kg of PTX) were peritumorally injected every two days. Two hours after injection, the tumor was locally irradiated by NIR laser and the temperature was maintained at 43–45 °C for 5 min. The volume of the tumors was measured and the body weight was monitored. At

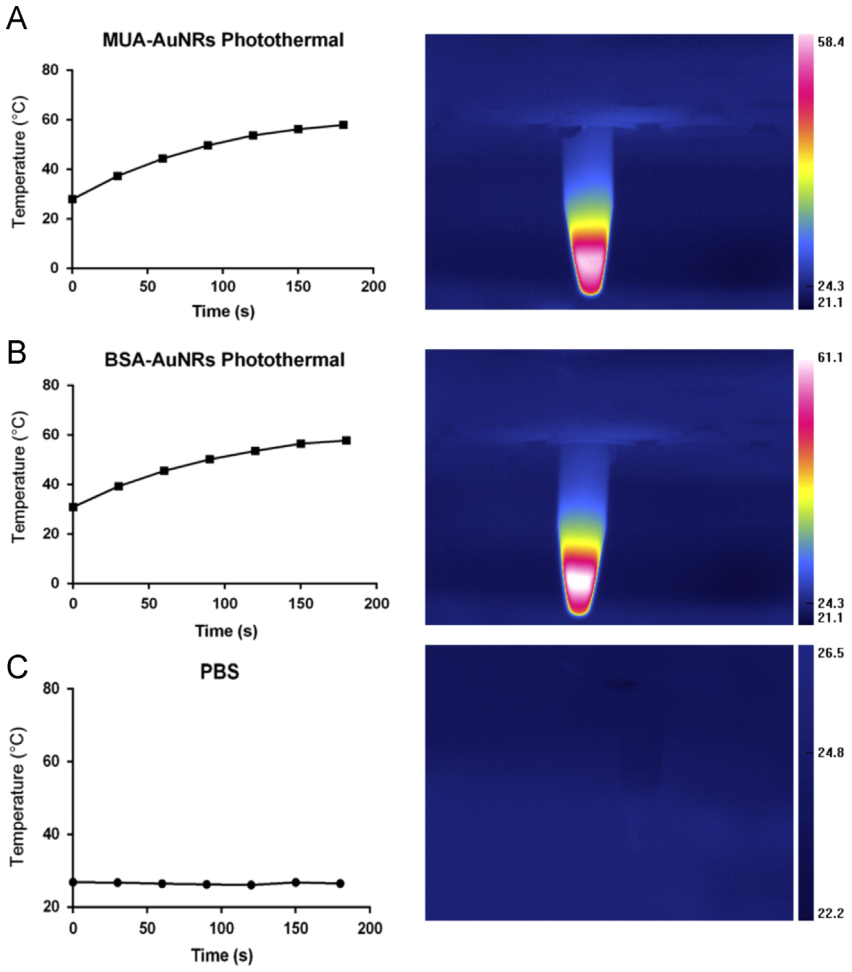

Figure 2 The photothermal effect of MUA-AuNRs (A), BSA-AuNRs (B), and PBS (C).

the end of the experiment, the tumors and major organs (heart, liver, spleen, lung, and kidney) were collected and weighted.

3. Results

3.1. Fabrication and Characterization of AuNRs

Seed synthesis is a classic method for preparation of AuNRs, with advantages, such as synthesis of convenience, high yield, and the precisely controlled LSPR. But this method typically involves the poorly biocompatible and cytotoxic CTAB. A further surface modification is generally required for *in vivo* application. In our study, by the ligand exchange method, the surface-coating CTAB was replaced by MUA. Subsequently, the MUA-AuNRs was modified with BSA, thus forming the improved biocompatible BSA-AuNRs. Moreover, PTX was encapsulated in the BSA-AuNRs *via* hydrophobic interaction (Scheme 1).

The morphology of AuNRs was observed using TEM, showing a size about 50 nm long and 10 nm wide (Fig. 1A). The zeta potential of the CTAB, MUA, and BSA-AuNRs was shown in Fig. 1B. The CTAB-AuNRs were positively charge (+ 36 mV), and the MUA-AuNRs and BSA-AuNRs were negative (–6.5 and –21.5 mV, respectively).

Gravimetric Analyzer (TGA) was used to characterize the composition ratio of the BSA-AuNRs (Fig. 1C). According to the thermogravimetric curve, the weight loss percentage of BSA was 74.91% and the BSA-AuNRs was 33.07%. Therefore, the BSA mass ratio of the BSA-AuNRs was calculated to be 36.15%.

The BSA-AuNRs displayed the improved colloidal stability at various pH, while the MUA-AuNRs aggregated at pH 3 (Fig. 1D–E). The BSA-AuNRs remained stable in either water and cell culture medium up to 4 days (Fig. 1F).

The photothermal properties of AuNRs were evaluated by measuring the temperature increase along with the time of laser exposure. The MUA-AuNRs or BSA-AuNRs in water (50 μg/mL) were illuminated, and the temperature of the MUA-AuNRs and BSA-AuNRs could rise to around 60 °C within 3 min (Fig. 2).

3.2. Cellular uptake of BSA-AuNRs, cytotoxicity of PTX/BSA-AuNRs and efficacy of photothermo-chemotherapy

The cellular uptake of BSA-AuNRs were enhanced, compared with the conventional PEG-AuNRs (Fig. 3A), presumably due to the albumin-binding proteins-mediated endocytosis. PTX was loaded in the BSA-AuNRs *via* hydrophobic interaction and the drug loading efficiency was 4.2%. The PTX/BSA-AuNRs as a chemotherapeutic agent was shown a high antitumor efficacy in the HCT116 cells, with an IC_{50} of 2 ng/mL, and that of the free PTX was 13.5 ng/mL for 72-h treatment (Fig. 3B). The enhanced antitumor activity could be due to the enhanced

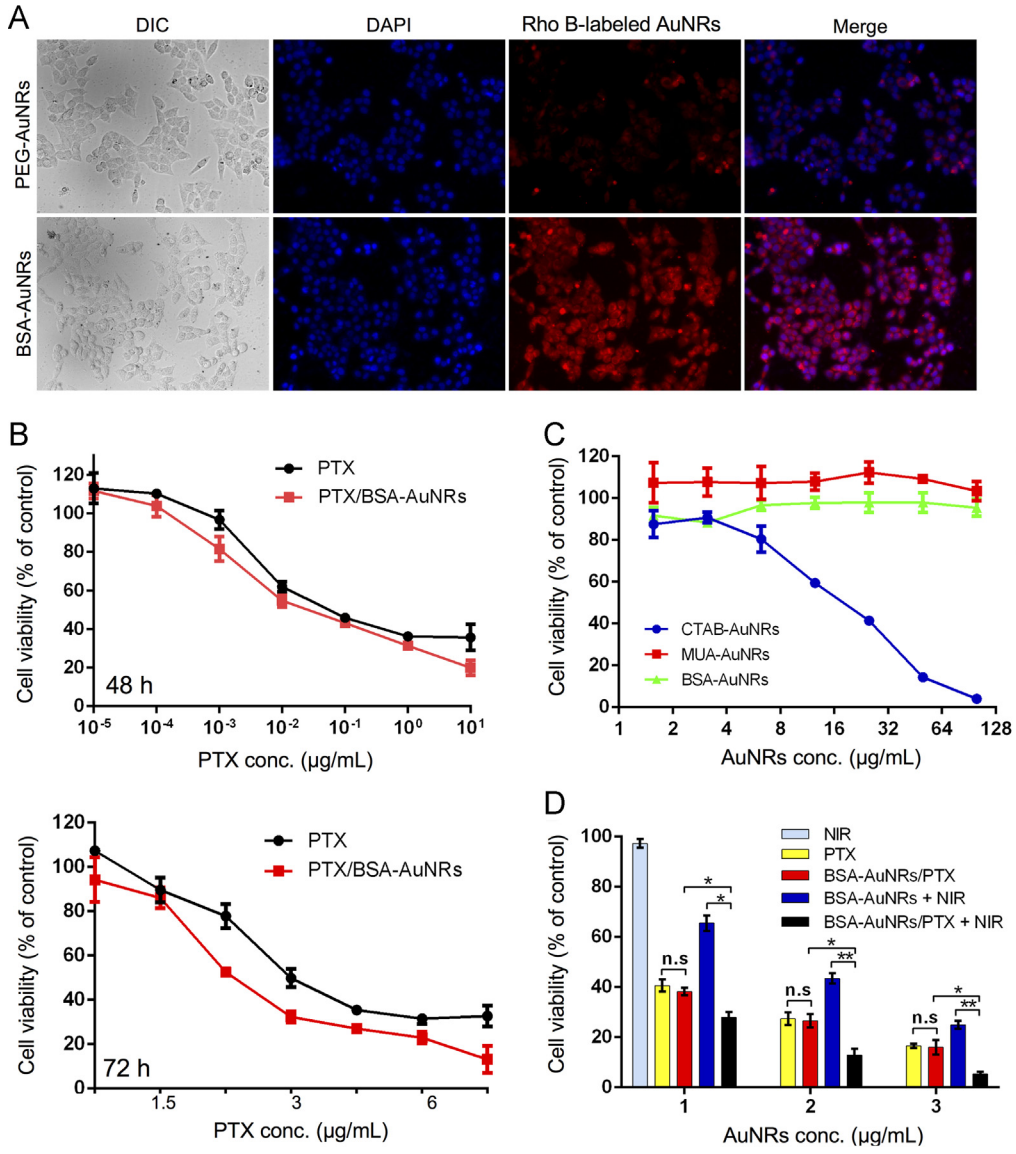

Figure 3 (A) Cellular uptake of BSA-AuNRs (scale bar: 50 μm); (B) Cytotoxicity of BSA-AuNRs/PTX and free PTX; (C) Cytotoxicity of the AuNRs with different surface coating; and (D) Antitumor activity of combined photothermo-chemotherapy.

cellular uptake. It should be pointed out that both the negatively charged AuNRs (MUA-AuNRs and BSA-AuNRs) displayed very good biocompatibility, compared to the highly cytotoxic CTAB-AuNRs (Fig. 3C).

The combination therapy was demonstrated by treating the cells with the PTX/BSA-AuNRs and the subsequent laser irradiation. Fig. 3D shows the cell viability of PTX, PTX/BSA-AuNRs, BSA-AuNRs + NIR, PTX/BSA-AuNRs + NIR were 16%, 15%, 20%, and 5%, respectively. It clearly demonstrated that combination therapy yielded a synergetic effect on killing the cancer cells.

3.3. *The effect on cell apoptosis and autophagy*

Both the single photothermal group (BSA-AuNRs + NIR) and the non-irradiation PTX/BSA-AuNRs could efficiently induce cell apoptosis, and the ratio of late apoptosis cells was 36.2% and 41.2%, respectively (Fig. 4A). Furthermore, the ratio in the combination group of PTX/BSA-AuNRs + NIR was enhanced to 52.2%, thus providing solid evidence for the benefits of the combination of photothermo-chemotherapy.

Autophagy is an important mechanism for antitumor therapy. LC3B is a key protein maker of cell autophagy, and its expression level can be used as an indicator of autophagy. Chloroquine phosphate that can strongly induce autophagy was set as a positive group. The autophagy level of in the PTX and PTX/BSA-AuNRs groups was relatively low, probably because PTX at the tested dose mainly induced cell apoptosis and its induction of cell autophagy was limited (Fig. 4B). However, the LC3B expression in both the photothermal groups was high, suggesting the efficient induction of autophagy. Interestingly, the autophagy level in the combination therapy declined compared to that of the single photothermal treatment. A possible explanation could be that the major action of PTX/BSA-AuNRs + NIR was the induction of apoptosis.

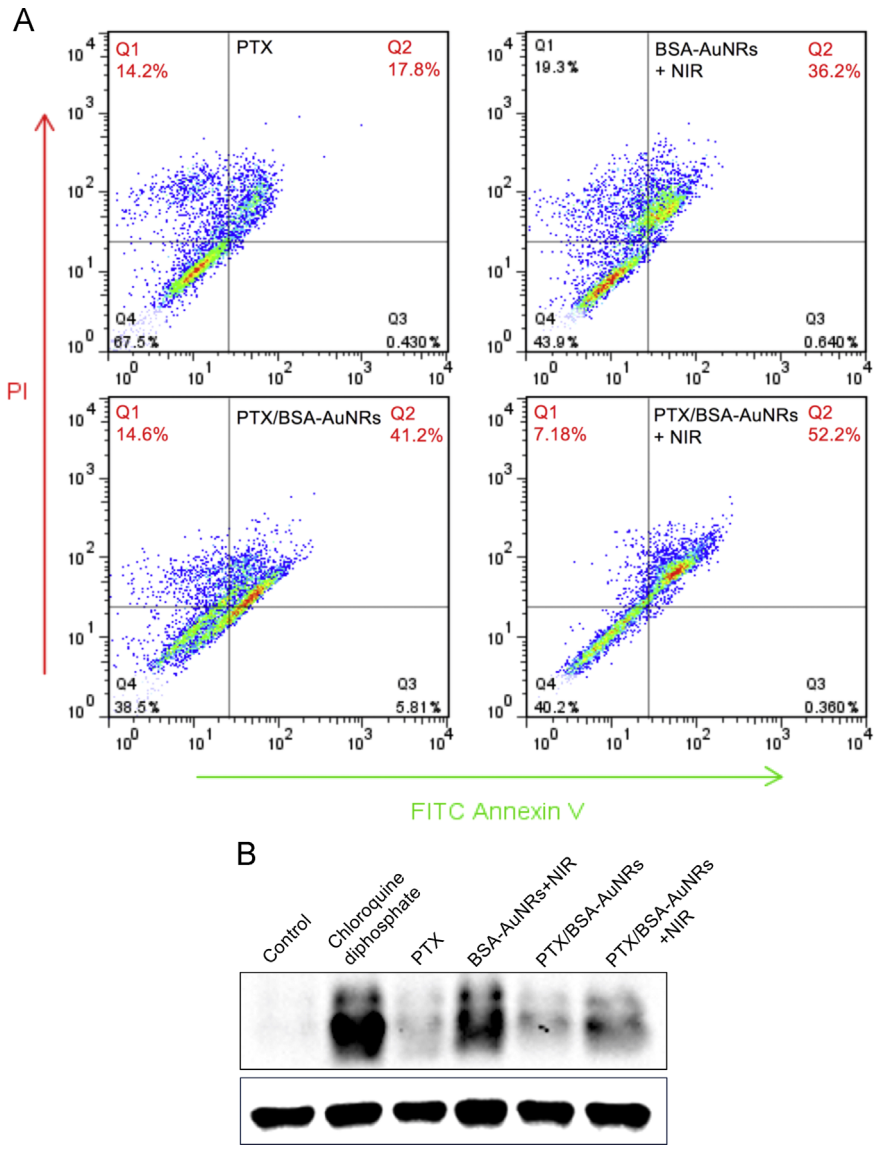

Figure 4 Pro-apoptosis effect (A) and autophagy (B) of photothermo-chemotherapy.

3.4. The effect of photothermal therapy on the classification of macrophages in vitro

Photothermotherapy on tumor cells has been reported that it can cause changes in gene expression and metabolism in many aspects. However, its effects on the tumor microenvironments (TME) largely remain unknown. Tumor-associated macrophages (TAM) are a major player in TME. TAMs are generally classified into two types: the antitumor M1 and pro-tumor M2 phenotypes. Polarization toward M2 phenotype promotes tumor progression, angiogenesis, and chemoresistance[22]. The increased infiltration of M2 macrophages in tumors is associated with drug resistance, and thus leads to chemotherapy failure. We have previously reported that suppression of the M2 polarization with a chemical modulator enhanced the chemotherapy efficacy in colon cancer and glioma[17,18]. Therefore, it was interesting to investigate the photothermal effect on TAM polarization. The mannose receptors (CD206) and the asparaginyl endopeptidase legumain are the often-used biomarkers to characterize the M2 phenotype TAM[23,24].

For the *in vitro* studies, the M2 phenotype was induced using IL-4. The expression of CD206 and legumain was remarkably downregulated after photothermal treatment with BSA/AuNRs, compared to the non-treatment group (Fig. 5). The suppression of M2 polarization by the BSA-AuNR-induced thermal effect was laser irradiation dose-dependent, and 3-min illumination showed the best inhibition effect than the other groups.

The induction of immune responses in tumors by photothermal therapy has been reported[25]. The mechanisms could be accounted for the production of the debris from the dead tumor cells caused by photothermotherapy served as the tumor antigens and elicited the cytotoxic T-cell effect. In this study, we discovered the immune cells (*e.g.*, TAMs) were also a part of the photothermotherapy-induced immune effects, *via* a mechanism of suppression of the TAM polarization toward M2 phenotype.

3.5. In vivo photothermo-chemotherapy

The treatment efficacy of the combined photothermo-chemotherapy was investigated using peritumoral administration as a pilot study. The peritumoral route could provide great convenience to

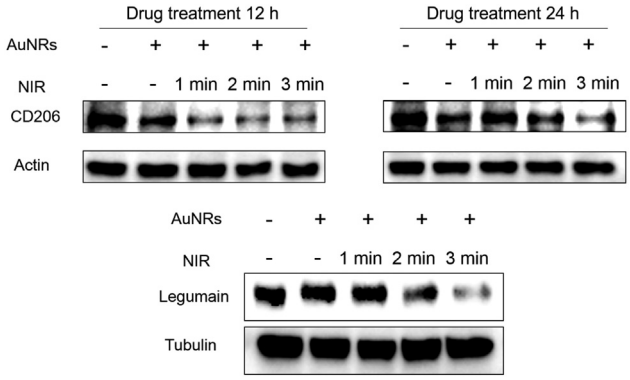

Figure 5 The suppression effect on the M2 polarization by photothermal therapy.

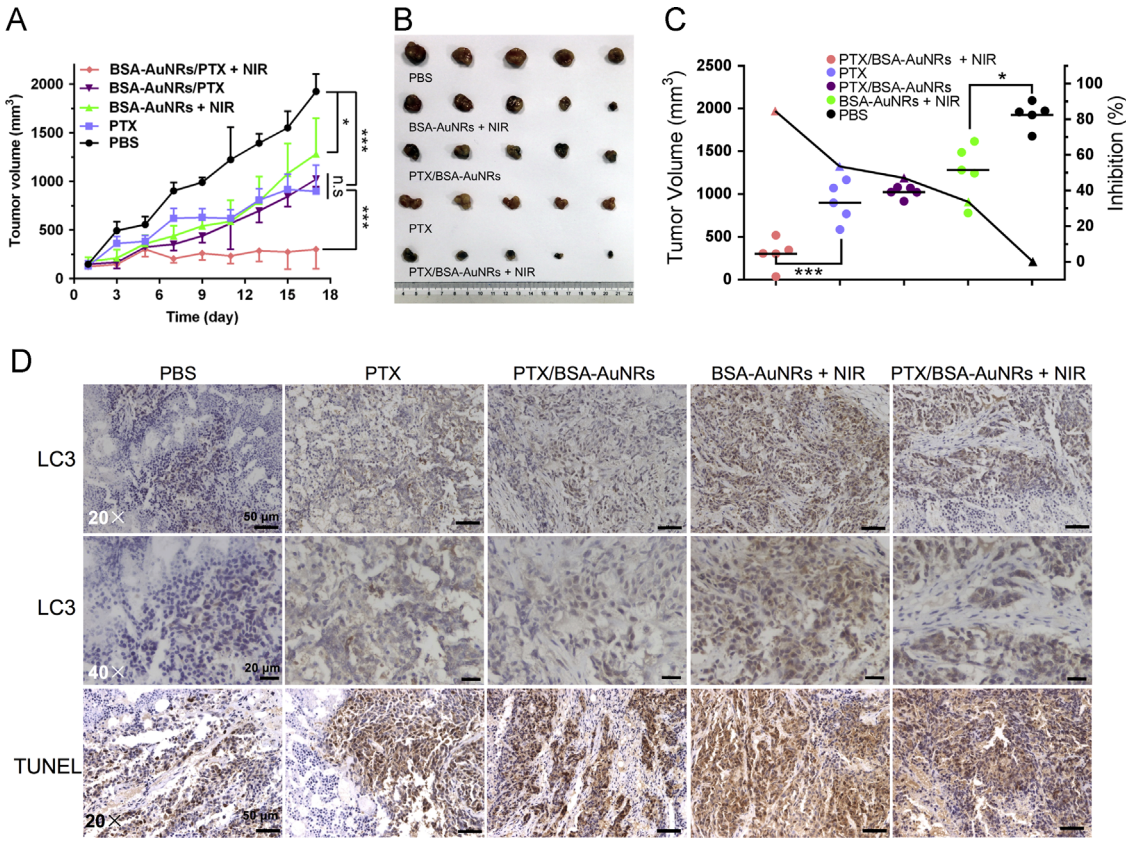

Figure 6 *In vivo* treatment efficiency. (A) Tumor volume change. (B) Tumor tissue images. (C) Tumor growth inhibition rate. (D) IHC staining of tumors to examine the expression of LC3 and TUNEL staining. Immunoperoxidase staining shows brown color.

examine the photothermal effect on TAM *in vivo*. The capacity of PTX/BSA-AuNRs to inhibit the tumor growth was demonstrated in the BALB/c nude mice bearing subcutaneous HCT116 colon tumors (Fig. 6A–C). The results showed that the tumors in the PBS-treated mice grew rapidly and the average tumor volume of 2000 mm^3 at day 17 (Fig. 6A). Both the chemotherapy alone (free PTX and PTX/BSA-AuNRs) and the photothermotherapy alone (BSA-AuNRs + NIR) showed moderate arrest of tumor growth. By sharp contrast, the photothermo-chemotherapy exhibited the strong inhibition of tumor growth, with an inhibition rate of 84.3% (Fig. 6C). The results demonstrated the synergetic effect of photothermo-chemotherapy.

At the end of the experiment, the tumors and major organs were dissected for further assay. Immunohistochemical (IHC) staining of tumors was performed to examine the LC3 expression. The TUNEL staining was also carried out to examine the apoptosis (Fig. 6D). LC3, the biomarker for autophagy, was highly expressed in the BSA-AuNRs + NIR group, which was consistent with that of the cell experiment. There were a large amount of apoptotic cells found in the BSA-AuNRs + NIR group. The amount of the M2-type macrophages, represented by the CD206 and legumain staining, was greatly reduced after the photothermo-chemotherapy (Fig. 7). It demonstrated that the combination successful re-educated the TAM and suppressed the polarization toward the pro-tumor M2 phenotype, thus activating

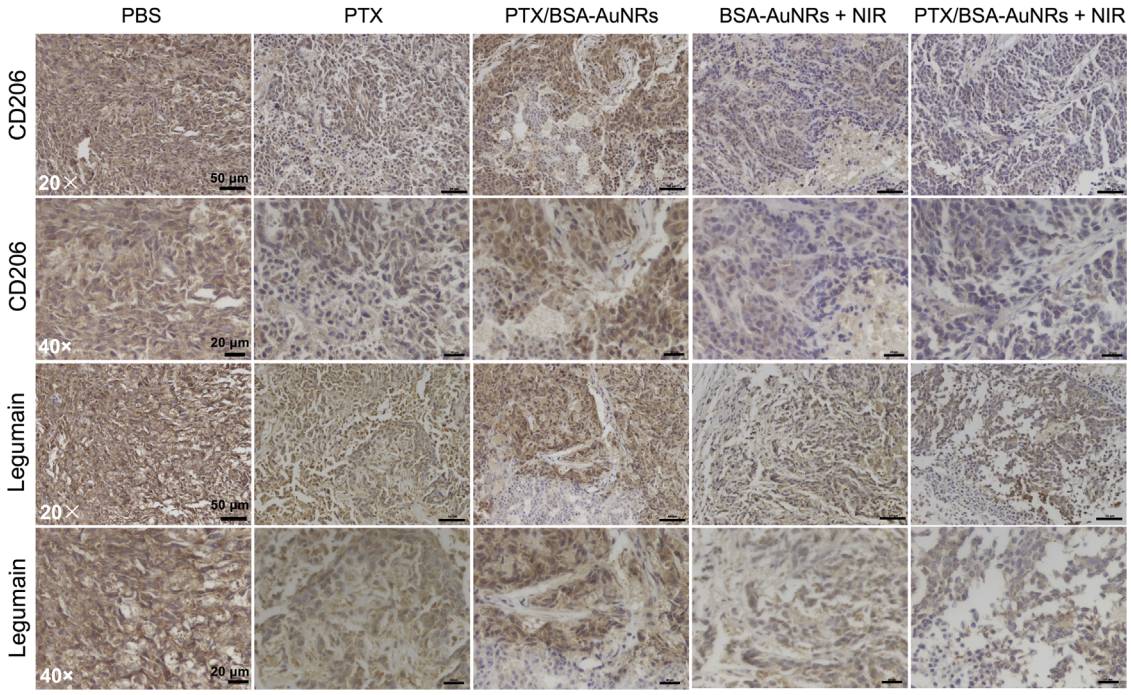

Figure 7 IHC staining of tumors to examine the expression of the M2 markers (CD 206 and legumain). Immunoperoxidase staining shows brown color.

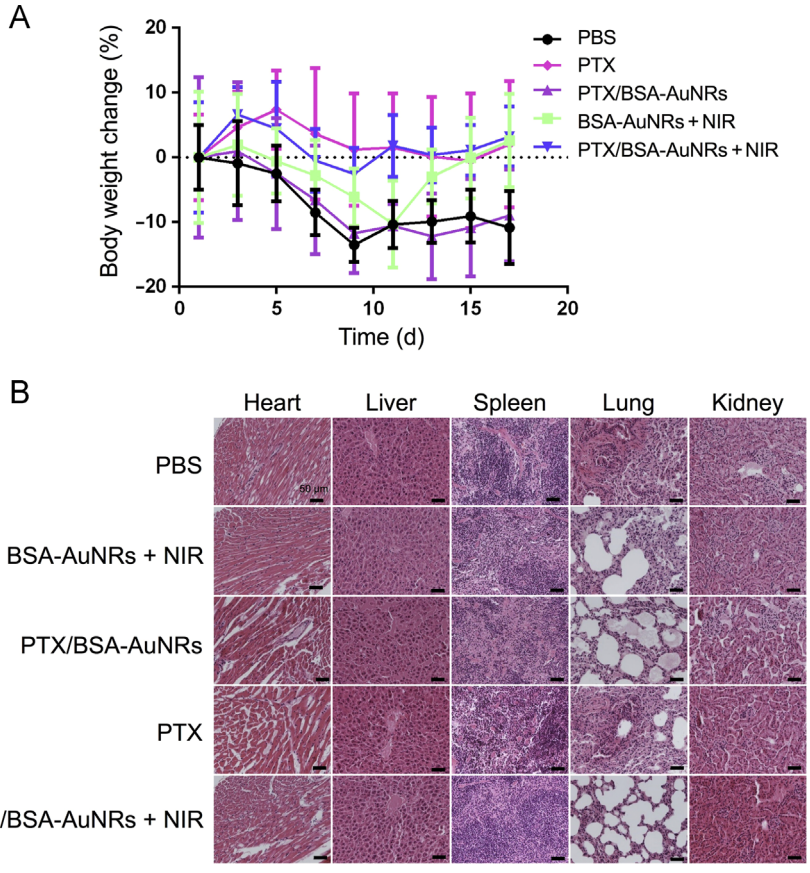

Figure 8 (A) Body weight change during the treatment course; (B) Histological examination of the major organs after treatment.

the immune system to kill the cancer cells. It could be a mechanism for photothermal immunotherapy.

The body weight change was shown in Fig. 8A, and the body weight of all the groups did not sustain significant change, indicating the safety of the treatments. Furthermore, the H&E histological examination showed there were no obvious damages (*e.g.*, degeneration or necrosis) in parenchymatous cells and no inflammatory in the major organs (*e.g.*, heart, liver, spleen, lung, and kidney) in the mice treated with the PTX/BSA-AuNRs + NIR (Fig. 8B).

4. Discussion

The major concern with photothermal application is the difficulty to direct heat specifically to the tumor region but sparing the normal tissue. However, its use in colorectal cancer would be promising because laser can be conveniently and precisely delivered to the tumor site *via* a fiber optic cable with endoscope. In fact, photodynamic therapy has been investigated in colorectal cancer in clinical practice with the aid of endoscopy[26].

The antitumor immunity elicited by photothermal treatment has been actively investigated[25]. It is generally believed that the immune responses can be induced by the release of the tumor antigens and the cell debris released by the local destruction of cancer cells by photothermal effect[25,27]. Our results demonstrated that redirecting the polarization of TAM was also a major immune mechanism. Of note, it has recently reported that phototherapy using high-fluency, low-power laser irradiation could mediate tumor-killing effect by inactivation of respiration chain oxidase, and which, interestingly, consequently induced phenotypic change of macrophages[28].

In cancer therapy, both innate immunity and acquired immunity play important roles. Macrophages-directed innate immunotherapy has been drawn great attention recently[29–31]. For example, M1 phenotype macrophages can secrete antitumor cytokines or directly "eat" the tumor cells. Therefore, the modulation of macrophages *via* a photothermal method is a promising target for cancer immunotherapy.

5. Conclusions

We developed the PTX/BSA-AuNRs for combining photothermal treatment with chemotherapy. The biomimetic modification with albumin not only improved the biocompatibility of the AuNRs but also enhanced the intracellular delivery *via* a mechanism of albumin-binding protein-mediated uptake. Additionally, the albumin hydrophobic domains could interact with PTX, thus serving as a drug–carrier albumin corona on the AuNRs. The synergistic effect of the photothermo-chemotherapy was demonstrated by both the *in vitro* and *in vivo* studies. The combination therapy yielded better efficacy than single treatment. Enhanced apoptosis was found in the combined therapy, while thermotherapy preferentially induced autophagy. More importantly, we discovered the photothermal treatment modulated the TME, and efficiently inhibited the polarization towards the M2 pro-tumor phenotype TAM. The animal studies demonstrated the combined therapy effectively arrested the tumor growth, yielding enhanced treatment outcomes with high biotolerance. In summary, this combination treatment provides a potential strategy for cancer therapy.

Acknowledgments

We thank the National Basic Research Program of China (973 Program 2014CB931900 and 2013CB932503) and NSFC, China (81373357, 81422048, 81673382 and 81521005) for the support. We also thank National Center for Protein Science Shanghai, CAS, for the technical support at Electron Microscopy Facility.

References

1 Park SE, Lee J, Lee T, Bae SB, Kang B, Huh YM, et al. Comparative hyperthermia effects of silica–gold nanoshells with different surface coverage of gold clusters on epithelial tumor cells. *Int J Nanomed* 2015;**10**:261–71.
2 Melancon MP, Lu W, Yang Z, Zhang R, Cheng Z, Elliot AM, et al. *In vitro* and *in vivo* targeting of hollow gold nanoshells directed at epidermal growth factor receptor for photothermal ablation therapy. *Mol Cancer Ther* 2008;**7**:1730–9.
3 Li Z, Huang P, Zhang X, Lin J, Yang S, Liu B, et al. RGD-conjugated dendrimer-modified gold nanorods for *in vivo* tumor targeting and photothermal therapy. *Mol Pharm* 2010;**7**:94–104.
4 Li Z, Huang H, Tang S, Li Y, Yu XF, Wang H, et al. Small gold nanorods laden macrophages for enhanced tumor coverage in photothermal therapy. *Biomaterials* 2016;**74**:144–54.
5 Nam J, Won N, Jin H, Chung H, Kim S. pH-induced aggregation of gold nanoparticles for photothermal cancer therapy. *J Am Chem Soc* 2009;**131**:13639–45.
6 Wang L, Wang L, Xu T, Guo C, Liu C, Zhang H, et al. Synthesis of 15P-conjugated PPy-modified gold nanoparticles and their application to photothermal therapy of ovarian cancer. *Chem Res Chin Univ* 2014;**30**:959–64.
7 Khan SA, Kanchanapally R, Fan Z, Beqa L, Singh AK, Senapati D, et al. A gold nanocage-CNT hybrid for targeted imaging and photothermal destruction of cancer cells. *Chem Commun* 2012;**48**:6711–3.
8 Wang Z, Chen Z, Liu Z, Shi P, Dong K, Ju E, et al. A multi-stimuli responsive gold nanocage-hyaluronic platform for targeted photothermal and chemotherapy. *Biomaterials* 2014;**35**:9678–88.
9 Chen H, Zhang X, Dai S, Ma Y, Cui S, Achilefu S, et al. Multifunctional gold nanostar conjugates for tumor imaging and combined photothermal and chemo-therapy. *Theranostics* 2013;**3**:633–49.
10 Li X, Xing L, Zheng K, Ping W, Du L, Shen M, et al. Formation of gold nanostar-coated hollow mesoporous silica for tumor multimodality imaging and photothermal therapy. *ACS Appl Mater Interfaces* 2017;**9**:5817–27.
11 Antaris AL, Robinson JT, Yaghi OK, Hong G, Diao S, Luong R, et al. Ultra-low doses of chirality sorted (6, 5) carbon nanotubes for simultaneous tumor imaging and photothermal therapy. *ACS Nano* 2013;**7**:3644–52.
12 Moon HK, Lee SH, Choi HC. *In vivo* near-infrared mediated tumor destruction by photothermal effect of carbon nanotubes. *ACS Nano* 2009;**3**:3707–13.
13 Ren F, Bhana S, Norman DD, Johnson J, Xu L, Baker DL, et al. Gold nanorods carrying paclitaxel for photothermal-chemotherapy of cancer. *Bioconjugate Chem* 2014;**24**:376–86.
14 You J, Zhang R, Xiong C, Zhong M, Melancon M, Gupta S, et al. Effective photothermal chemotherapy using doxorubicin-loaded gold nanospheres that target EphB4 receptors in tumors. *Cancer Res* 2012;**72**:4777–86.
15 Wang X, Zhang J, Wang Y, Wang C, Xiao J, Zhang Q, et al. Multi-responsive photothermal-chemotherapy with drug-loaded melanin-like nanoparticles for synergetic tumor ablation. *Biomaterials* 2016;**81**:114–24.
16 Desai NP, Trieu V, Hwang LY, Wu R, Soon-Shiong P, Gradishar WJ. Improved effectiveness of nanoparticle albumin-bound (*nab*) paclitaxel

versus polysorbate-based docetaxel in multiple xenografts as a function of HER2 and SPARC status. *Anticancer Drugs* 2008;**19**:899–909.
17 Zhao P, Yin W, Wu A, Tang Y, Wang J, Pan Z, et al. Dual-targeting to cancer cells and M2 macrophages *via* biomimetic delivery of mannosylated albumin nanoparticles for drug-resistant cancer therapy. *Adv Funct Mater* 2017. Available from: http://dx.doi.org/10.1002/adfm.201700403.
18 Lin T, Zhao P, Jiang Y, Tang Y, Jin H, Pan Z, et al. Blood–brain-barrier-penetrating albumin nanoparticles for biomimetic drug delivery *via* albumin-binding protein pathways for antiglioma therapy. *ACS Nano* 2016;**10**:9999–10012.
19 Wang C, Xu L, Liang C, Xiang J, Peng R, Liu Z. Immunological responses triggered by photothermal therapy with carbon nanotubes in combination with anti-CTLA-4 therapy to inhibit cancer metastasis. *Adv Mater* 2014;**26**:8154–62.
20 Mirza AZ. A novel drug delivery system of gold nanorods with doxorubicin and study of drug release by single molecule spectroscopy. *J Drug Target* 2015;**23**:52–8.
21 Wijaya A, Hamad-Schifferli K. Ligand customization and DNA functionalization of gold nanorods *via* round-trip phase transfer ligand exchange. *Langmuir* 2008;**24**:9966–9.
22 Chanmee T, Ontong P, Konno K, Itano N. Tumor-associated macrophages as major players in the tumor microenvironment. *Cancers (Basel)* 2014;**6**:1670–90.
23 Smahel M, Duskova M, Polakova I, Musil J. Enhancement of DNA vaccine potency against legumain. *J Immunother* 2014;**37**:293–303.
24 Luo Y, Zhou H, Krueger J, Kaplan C, Lee SH, Dolman C, et al. Targeting tumor-associated macrophages as a novel strategy against breast cancer. *J Clin Investig* 2006;**116**:2132–41.
25 Chen Q, Xu L, Liang C, Wang C, Peng R, Liu Z. Photothermal therapy with immune-adjuvant nanoparticles together with checkpoint blockade for effective cancer immunotherapy. *Nat Commun* 2016;**7**:13193.
26 Kawczyk-Krupka A, Bugaj AM, Latos W, Zaremba K, Wawrzyniec K, Sieroń A. Photodynamic therapy in colorectal cancer treatment: the state of the art in clinical trials. *Photodiagnosis Photodyn Ther* 2015;**12**:545–53.
27 Zhou F, Nordquist RE, Chen WR. Photonics immunotherapy–a novel strategy for cancer treatment. *J Innov Opt Health Sci* 2015;**9**:1630001.
28 Lu C, Zhou F, Wu S, Liu L, Xing D. Phototherapy-induced antitumor immunity: long-term tumor suppression effects *via* photoinactivation of respiratory chain oxidase-triggered superoxide anion burst. *Antioxid Redox Signal* 2016;**24**:249–62.
29 Mills CD, Lenz LL, Harris RA. A breakthrough: macrophage-directed cancer immunotherapy. *Cancer Res* 2016;**76**:513–6.
30 Alvey CM, Spinler KR, Irianto J, Pfeifer CR, Hayes B, Xia Y, et al. SIRPA-inhibited, marrow-derived macrophages engorge, accumulate, and differentiate in antibody-targeted regression of solid tumors. *Curr Biol* 2017;**27**(2065-77)e6.
31 Gholamin S, Mitra SS, Feroze AH, Liu J, Kahn SA, Zhang M, et al. Disrupting the CD47-SIRPα anti-phagocytic axis by a humanized anti-CD47 antibody is an efficacious treatment for malignant pediatric brain tumors. *Sci Transl Med* 2017;**9**:eaaf2968.